IEEE Access
Multidisciplinary ⋮ Rapid Review ⋮ Open Access Journal

Received December 6, 2020, accepted December 14, 2020, date of publication December 17, 2020,
date of current version December 30, 2020.

Digital Object Identifier 10.1109/ACCESS.2020.3045464

A Deep Learning-Based Approach for Radiation Pattern Synthesis of an Array Antenna

JAE HEE KIM[1], (Senior Member, IEEE), AND SANG WON CHOI[2], (Member, IEEE)
[1]School of Electrical, Electronics and Communication Engineering, Korea University of Technology and Education, Cheonan 31253, South Korea
[2]Department of Electronic Engineering, Kyonggi University, Suwon 16227, South Korea

Corresponding author: Sang Won Choi (swchoi20@kyonggi.ac.kr)

This work was supported by the Education and Research Promotion Program of KOREATECH in 2020.

ABSTRACT In this article, we propose a deep neural network (DNN)- for the radiation pattern synthesis of an antenna. The DNN utilizes the radiation patterns as inputs and the amplitude and phase of the antenna elements as outputs. Consequently, the radiation patterns of the array antenna can be easily obtained from the outputs of the trained DNN, which are amplitude and phase of the antenna elements. However, it is difficult to determine the amplitude and phase of each antenna element from the desired pattern in an environment where inter-element coupling exists. For this purpose, 6,859 radiation pattern samples for a 4×1 array patch antenna were generated by changing the phases of the antenna elements, and those patterns were leveraged to train the proposed DNN with low complexity. The radiation patterns of the ideal square and triangular array shapes, which are practically infeasible to implement, were used as inputs to the DNN. It was confirmed that the radiation pattern generated from the output signals of the DNN was very similar to the input radiation pattern.

INDEX TERMS Antenna, deep learning, neural network, radiation patterns, synthesis.

I. INTRODUCTION

The radiation pattern of an array antenna is determined by the amplitude and phase of the signal applied to each antenna element [1]. In actual array antennas, there is coupling between the various antenna elements. Consequently, it is difficult to determine the signal amplitude and phase for each array elements in order to obtain the desired array radiation pattern. As a typical approach, Fourier transform or optimization techniques can be utilized to synthesize the radiation pattern of the array antenna [2]–[4]. However, these methods cannot be easily implemented in practice, and the synthesis of even a single radiation pattern requires a considerable amount of computation time. To synthesize different types of radiation patterns for the same antenna structure, the algorithm must be re-operated several times for each pattern, resulting in even longer computation time.

Recently, deep learning (DL) has been applied to various research fields and applications, including electromagnetic (EM) problems. The DL approach has also been utilized to design and synthesize various types of antennas [5]–[6]. While designing the antenna structure, the simulation time could be reduced by replacing EM simulations with DL methodology [7], [8]. Furthermore, to improve the antenna's performance, a DL approach has been studied for antenna pattern synthesis, fault diagnosis, and far-field imaging [9]–[16].

From the perspective of implementation, the distortion of the radiation pattern, due to coupling, becomes more pronounced where the distance between the elements of the array antenna become smaller. To minimize the side effects of coupling, a neural network (NN)-based methodology was studied for radiation pattern synthesis [5], [10]. When the antenna elements fail in an array antenna, the radiation pattern is changed. To diagnose the failure of antenna elements, a convolutional NN (CNN) has been used in conjunction with the input radiation pattern [11]. In addition, the CNN has been used to determine the excitation signal of the antenna element [9], [14]. As the study for antenna synthesis, based on CNN, shed light on the feasibility of DNN as a reasonable candidate for learning arbitrary antenna radiation patterns, we therefore propose a DL based methodology to estimate the excitation signal by interpreting the radiation pattern as a corresponding image.

The main contribution of this article is to provide a DL methodology that derives and outputs the amplitude and phase of the antenna elements in response to an ideal input

The associate editor coordinating the review of this manuscript and approving it for publication was Bilal Khawaja.

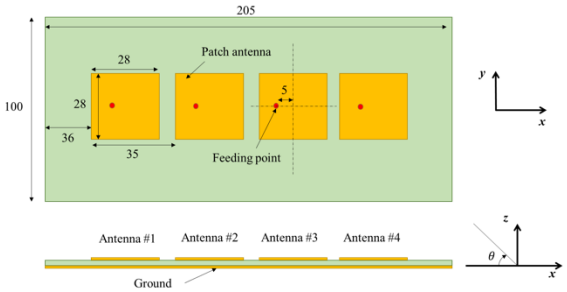

FIGURE 1. Array antenna structure used for radiation pattern simulations.

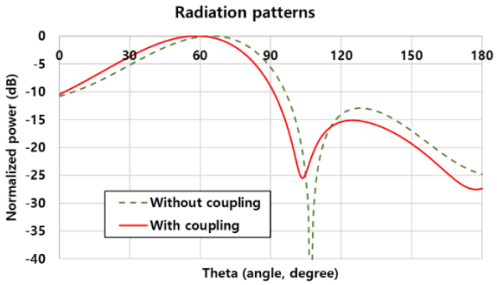

FIGURE 2. Comparison of radiation patterns with or without coupling.

radiation pattern. While the previous work was to seek the amplitude and phase of an antenna for the attainable radiation pattern, the proposed methodology is utilized to search for the signals to provide the desired radiation pattern. The proposed methodology can also be directly applied to determine the amplitude and phase for various radiation patterns once these have been learned via DNN training and validation. In Section II, the structure of the array antenna is described. Section III presents the radiation pattern data for deep learning. Section IV describes the deep neural network. The applications of the deep learning outcomes are described in Section V. The conclusions are presented in Section VI.

II. ARRAY PATTERN STRUCTURE

Fig. 1 describes the antenna structure for the simulation of the radiation pattern corresponding to the input signal of the antenna element. A 4×1 array antenna was designed, and a patch antenna was used as the antenna element. An FR4 substrate with a dielectric constant of 4.3 and a thickness of 1 mm was used. The patch antennas had the same length and width (28×28 mm). The feeding point was 5 mm to the left of the center of the patch antenna. The operating frequency of the antenna was 2.4 GHz. To investigate the effect of deep learning, a high coupling between the array antenna elements was chosen with the distance between antennas being equal to 0.28 λ (35 mm). This is narrower than 0.5 λ, typically used in array antennas.

The radiation pattern of an array antenna, without coupling, can be expressed simply as the product of the radiation pattern of a single antenna and an array factor. However, in the case of the array antenna, with coupling, the radiation pattern is distorted by the coupling. Fig. 2 compares the simulated radiation patterns with and without coupling. The amplitude and phase of the input signals of the antenna elements in Fig. 1 are as follows: antenna #1: $1\angle 0°$, antenna #2: $1\angle 60°$, antenna #3: $1\angle 120°$, and antenna #4: $1\angle 180°$.

The simulations were performed using ANSYS and HFSS (commercial three-dimensional EM software). The radiation pattern, without coupling, was obtained by multiplying the radiation pattern of a single patch antenna by an array factor. The radiation pattern, with coupling, was simulated by directly inputting a signal with a phase difference of 60° to each antenna element. As shown in the simulation results, the coupling distorts the radiation patterns. Therefore, it is necessary to find the amplitude and phase of the signal to obtain a radiation pattern without the effects of coupling. This can be obtained by using various algorithms. A DL methodology is used to determine the amplitude and phase of the signal required to synthesize the antenna radiation pattern for the case where the coupling exists.

TABLE 1. Amplitude and Phase of Antenna Input Signals for the Training Set.

	Amplitude	Phase	Number of cases
Antenna #1	1	0°	1
Antenna #2	1	0°, 20°, 40°, 60°, … 340°, 360°	19
Antenna #3	1	0°, 20°, 40°, 60°, … 340°, 360°	19
Antenna #4	1	0°, 20°, 40°, 60°, … 340°, 360°	19

III. EXTRACTION OF RADIATION PATTERN DATA

The radiation pattern was mainly determined by the phase of the signal that excited the antenna element. The radiation patterns were acquired while the phase of the signals were varied. The relative phase difference was more important than the absolute phase value of each antenna. Therefore, the phase of antenna #1 was fixed at 0°, and the phase of the other antennas were compared with it. The radiation patterns of the training data were acquired by increasing the phase by 20°. As shown in Table 1, the number of cases created per antenna is 19; thus, the total number of radiation patterns is $1 \times 19 \times 19 \times 19 = 6,859$. To verify whether the deep neural network is properly trained, validation data should not overlap with the training data. Table 2 lists the validation data. The initial phase started from 10°, increased by 40°, and stopped at 130°. Because the number of cases made per antenna was four, the total number of radiation patterns was $1 \times 4 \times 4 \times 4 = 64$.

The radiation patterns were extracted with MATLAB and HFSS. In MATLAB, the amplitude and phase of the signals were specified as variables and the values given in Tables I and II were assigned to the variables. The antenna structure shown in Fig. 1 was simulated and saved once using HFSS. The previously simulated HFSS file was opened with MATLAB. The amplitude and phase variables of the antenna were input to HFSS, and the radiation pattern was extracted. These patterns were two-dimensional, and their values were

TABLE 2. Amplitude and Phase of Antenna Input Signals for the Validation Set.

	Amplitude	Phase	Number of cases
Antenna #1	1	0°	1
Antenna #2	1	10°, 50°, 90°, 130°	4
Antenna #3	1	10°, 50°, 90°, 130°	4
Antenna #4	1	10°, 50°, 90°, 130°	4

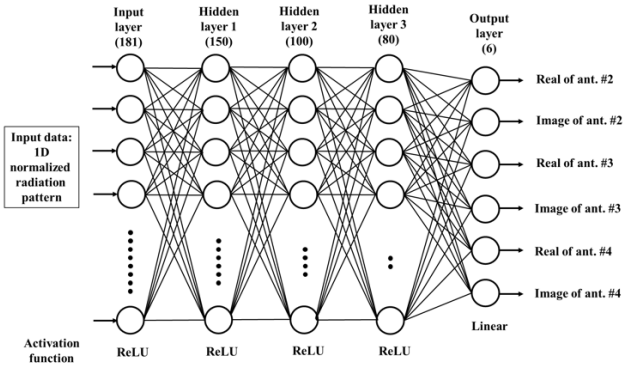

FIGURE 3. Architecture of the deep neural network.

extracted in units of 1° according to the θ value in Fig. 1. The starting point was 0°, and the maximum value was 180°. The radiation pattern corresponds to the E-plane of the patch antenna.

IV. NEURAL NETWORK MODELING AND TRAINING

A DNN was constructed, as shown in Fig. 3. It is very important to determine the type of input and output of the DNN. This is because learning results can be completely dependent on the type of input and output data. The radiation patterns were extracted in units of 1° according to the θ value ranging from 0° to 180°. In general, the intensity of the radiation pattern was expressed in dB; however, as the input data must be normalized, the dimension of the radiation pattern was converted to a scalar value. The number of input data was 181, and their values ranged from zero to one.

When the phase of the signal was set as the DNN output data, there were two different outputs for one input due to 0° and 360° being equivalent values. As this may result in poor learning, the DNN output data, amplitude and phase, were expressed as complex numbers. For example, using real and imaginary values to output data, a signal with an amplitude of one and a phase of 45° can be expressed as $1e^{j\pi/4} = 0.707 + j0.707$. The output of the DNN has a real part of 0.707 and an imaginary part of 0.707.

The configuration of the DNN is shown in Fig. 3. The DNN consists of five layers. The activation function of the last layer is the "linear" function with the remaining layers using the "rectified linear unit (ReLU)" function to overcome the vanishing gradient problem. Each layer uses a dense layer that fully connected both input and output neurons. As the depth of the network increased, the number of output neurons was reduced. The loss function used to compile the DNN was

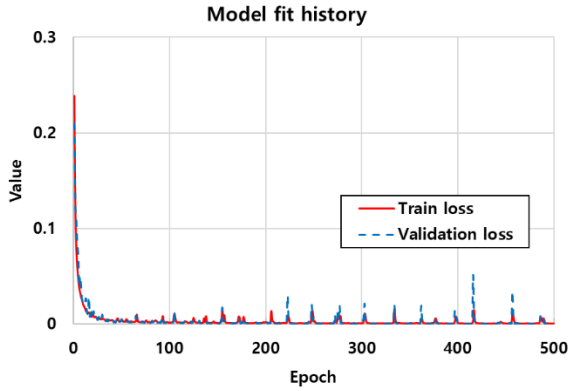

FIGURE 4. Train and validation losses as a function of epoch.

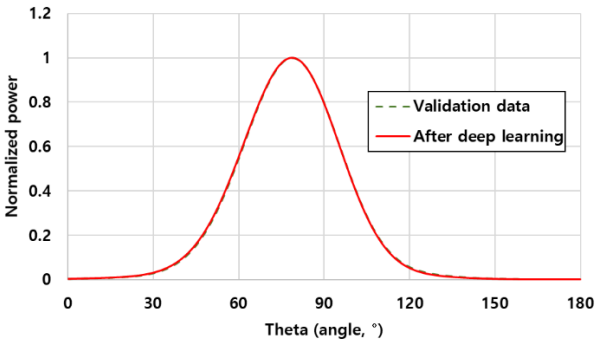

FIGURE 5. Deep learning data verification using one sample of the validation set.

used in conjunction with a mean squared error. The Adam optimizer was used. For training, 6,859 radiation patterns corresponding to Table 1 were used. In Table 2, 64 radiation patterns were used as validation data. The epochs were set to 500 for training 500 times. The batch size was set to 100. TensorFlow 2.0 was used for the simulations. The loss according to the epoch is shown in Fig. 4. It can be observed that the value converges as the epoch increases. The final converged train loss was 0.00022, and the validation loss was 0.00026. It took approximately 3 min to train the DNN when using the hardware specification of Intel(R) Xeon(R) CPU @ 2.30 GHz with a memory of 16 GB.

V. SIMULATION RESULTS

To validate the DNN output data, one of the validation sets was selected and compared. The phase of the array antenna in the validation data was selected as follows: antenna #1: $1\angle 0°$, antenna #2: $1\angle 50°$, antenna #3: $1\angle 10°$, and antenna #4: $1\angle 90°$.

For the above data, the radiation pattern ("validation data" in Fig. 5) was obtained through simulation with HFSS. The pattern was then used as the input dataset of the DNN, and the output data were obtained. The output data are as shown in Table 3.

It is observed that the DNN output data are almost similar to the output data of the validation set. The radiation pattern ("after deep learning" in Fig. 5) was obtained through HFSS

TABLE 3. Output Data of DNN for the Validation Sample.

	Real	Imaginary	Amplitude/Phase
Antenna #1	1	0	$1\angle 0°$
Antenna #2	0.64042646	0.7917143	$1.02\angle 51.0302°$
Antenna #3	0.99693894	0.21536693	$1.02\angle 12.1902°$
Antenna #4	−0.00635789	1.0284995	$1.03\angle 90.3542°$.

TABLE 4. Output Data of DNN for the Square Pattern.

	Real	Imaginary	Amplitude/Phase
Antenna #1	1	0	$1\angle 0°$
Antenna #2	−0.95035845	−0.71866751	$1.19\angle -142.9032°$
Antenna #3	0.69105726	−1.4455540	$1.60\angle -64.4495°$
Antenna #4	−1.3081744	−0.063080259	$1.31\angle -177.2393°$

TABLE 5. Output Data of DNN for the Triangular Pattern.

	Real	Imaginary	Amplitude/Phase
Antenna #1	1	0	$1\angle 0°$
Antenna #2	−1.2710851	0.82223773	$1.51\angle 147.1020°$
Antenna #3	0.67788279	0.052280359	$0.67\angle 4.4101°$
Antenna #4	−0.98690575	−0.34272450	$1.04\angle -160.8493°$

simulations by using the DNN output data. The two radiation patterns are compared and presented in Fig. 5. It can be observed that the two radiation patterns appear almost identical. In other words, the phase value of the array antenna obtained by inputting the radiation pattern is appropriate.

By leveraging the learned DNN via training and validation, a radiation pattern that is difficult to predict was input to determine the phase of the array antenna. An ideal radiation pattern, which could not be generated from the array antenna, was used as an input value. Fig. 6(a) depicts an ideal square input pattern with a gain of one within the angular range of 100–140° and a gain of 0.001 for all other angles. When the square-shaped radiation pattern was input, the DNN displayed the output as shown in Table 4. The DNN output was used as input signals of the array antenna, as shown in Fig. 1, and the radiation pattern was simulated. The radiation pattern is marked as "After deep learning" in Fig. 6(a). The radiation pattern exhibits a maximum gain at 114° and a similar waveshape to the input pattern of the DNN.

An ideal triangular shape was also inserted into the DNN. The shape of the input data is shown as an "input pattern" in Fig. 6(b). The output value of the DNN is shown in Table 5. The radiation pattern was simulated based on the outputs of the DNN, and the pattern is depicted as "after deep learning" in Fig. 6(b). This is quite similar to the input shape. Because the input pattern is not realistic, the solution cannot match completely. However, the DNN presented an output value that could produce a result similar to the desired radiation pattern.

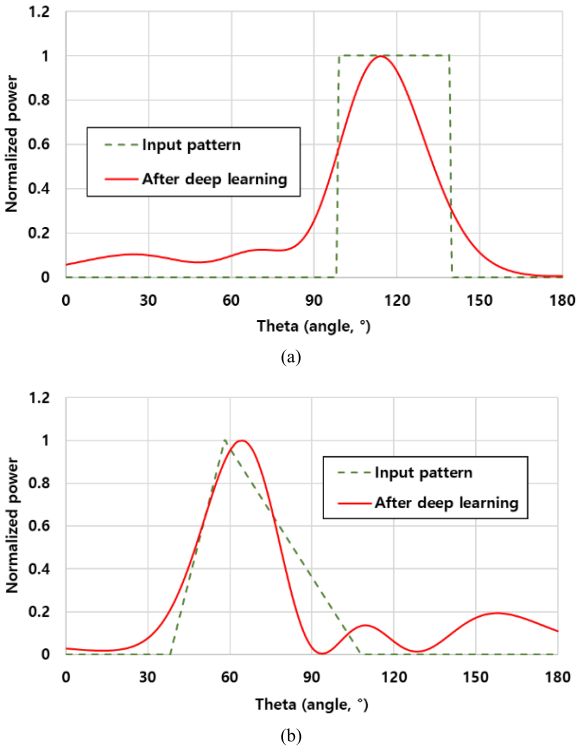

FIGURE 6. Radiation pattern synthesis according to the input of an arbitrary ideal pattern: (a) square and (b) triangular shapes.

TABLE 6. Comparison of the Different ML Architecture for Pattern Synthesis.

Reference	Application	NN size	Architecture
[9]	2D Synthesis of Reflectarray	8	CNN
[14]	2D Pattern synthesis	7	CNN
[Proposed]	1D Pattern synthesis	5	DNN

Therefore, DNN can play a useful role for synthesizing desired radiation patterns.

VI. DISCUSSION

The feasibility of radiation pattern synthesis has been shown by several NN methodologies, such as NN and support vector machine [5]. However, for such machine learning engines, there is an inherent limitation on learning different antenna radiation patterns. In other words, NNs without using deep hidden layers might not provide antenna design parameters for an arbitrary antenna radiation pattern. For that, the proposed DNN can be utilized along with dealing with practical issues such as the coupling effect. The determination of whether there is a limit to using the proposed DNN in the case of extreme coupling would be a valuable research direction in future.

Another important aspect is that the use of the proposed DNN is different from the conventional use of the CNN. Specifically, convolution filter and max pooling

which are main components of the CNN are not used. In [9], [14], the radiation pattern was imaged by introducing the well-defined CNN, and the pattern was synthesized from this image. However, since all of the outputs are used as phase values, there is a possibility that learning for phase information near 0° and 360° may not work well. Moreover, validation was performed only for the radiation pattern that can be actually obtained.

The prominent difference of the proposed DNN from the conventional schemes is that it utilizes real and imaginary numbers instead of the phase value in order to enhance the ability of learning for an arbitrary antenna radiation pattern. By numerical validation, it was observed that reasonable antenna parameters, for antenna synthesis, can be provided even for an antenna radiation pattern that cannot be derived easily in the practical sense.

VII. CONCLUSION

A deep learning-based methodology was designed to synthesize the radiation pattern of array antennas. In order to derive the radiation patterns, including the case where coupling exists between the antenna elements, a 4×1 array patch antenna with a spacing of $0.28\ \lambda$ was utilized. A DNN was then constructed with the input being the radiation pattern and the output being the amplitude and phase of the antenna. It was shown that the proposed DNN trained (validated) by 6,859 (64) radiation pattern samples exhibits reasonable performance in synthesizing the corresponding radiation patterns. Based on the test results of the proposed DNN with a low complexity, it was observed that the deep learning is feasible for the ideal radiation patterns of square and triangular shapes. The results validated that the radiation pattern from the DNN outputs were quite similar to the input radiation pattern. This demonstrated that deep learning can be used reliably for radiation pattern synthesis. As a future work, the feasibility of the DNN-based methodology can be extended for strongly coupled MIMO antennas implemented inside a mobile phone.

REFERENCES

[1] C. A. Balanis, *Antenna Theory: Analysis and Design*, vol. 1. Hoboken, NJ, USA: Wiley, 2005.

[2] Z. He, Z. Hua, L. Hongmei, L. Beijia, and W. Qun, "Array antenna pattern synthesis method based on intelligent algorithm," in *Proc. IEEE Int. Conf. Electron. Inf. Commun. Technol. (ICEICT)*, Harbin, China, Aug. 2016, pp. 549–551.

[3] D. Hua, W. Wu, and D.-G. Fang, "The synthesis of a magneto-electric dipole linear array antenna using the element-level pattern diversity (ELPD) technique," *IEEE Antennas Wireless Propag. Lett.*, vol. 17, no. 6, pp. 1069–1072, Jun. 2018.

[4] J. L. Gomez-Tornero, A. J. Martinez-Ros, and R. Verdu-Monedero, "FFT synthesis of radiation patterns with wide nulls using tapered leaky-wave antennas," *IEEE Antennas Wireless Propag. Lett.*, vol. 9, pp. 518–521, May 2010.

[5] H. M. E. Misilmani and T. Naous, "Machine learning in antenna design: An overview on machine learning concept and algorithms," in *Proc. Int. Conf. High Perform. Comput. Simulation (HPCS)*, Dublin, Ireland, Jul. 2019, pp. 600–607.

[6] D. Erricolo, P.-Y. Chen, A. Rozhkova, E. Torabi, H. Bagci, A. Shamim, and X. Zhang, "Machine learning in electromagnetics: A review and some perspectives for future research," in *Proc. Int. Conf. Electromagn. Adv. Appl. (ICEAA)*, Granada, Spain, Sep. 2019, pp. 1377–1380.

[7] C. Gianfagna, H. Yu, M. Swaminathan, R. Pulugurtha, R. Tummala, and G. Antonini, "Machine-learning approach for design of nanomagnetic-based antennas," *J. Electron. Mater.*, vol. 46, no. 8, pp. 4963–4975, Apr. 2017.

[8] J. Tak, A. Kantemur, Y. Sharma, and H. Xin, "A 3-D-PrintedW-Band slotted waveguide array antenna optimized using machine learning," *IEEE Antennas Wireless Propag. Lett.*, vol. 17, no. 11, pp. 2008–2012, Nov. 2018.

[9] T. Shan, M. Li, S. Xu, and F. Yang, "Synthesis of refiectarray based on deep learning technique," in *Proc. Cross Strait Quad-Regional Radio Sci. Wireless Technol. Conf. (CSQRWC)*, Xuzhou, China, Jul. 2018, pp. 1–2.

[10] R. G. Ayestaran, F. Las-Heras, and L. F. Herran, "High-accuracy neural-network-based array synthesis including element coupling," *IEEE Antennas Wireless Propag. Lett.*, vol. 5, pp. 45–48, Mar. 2006.

[11] Q. Chen, H. Ma, and E.-P. Li, "Failure diagnosis of microstrip antenna array based on convolutional neural network," in *Proc. IEEE Asia–Pacific Microw. Conf. (APMC)*, Singapore, Dec. 2019, pp. 90–92.

[12] M. H. Nielsen, M. H. Jespersen, and M. Shen, "Remote diagnosis of fault element in active phased arrays using deep neural network," in *Proc. 27th Telecommun. Forum (TELFOR)*, Belgrade, Serbia, Nov. 2019, pp. 1–4.

[13] T. N. Kapetanakis, I. O. Vardiambasis, M. P. Ioannidou, and A. Maras, "Neural network modeling for the solution of the inverse loop antenna radiation problem," *IEEE Trans. Antennas Propag.*, vol. 66, no. 11, pp. 6283–6290, Nov. 2018.

[14] R. Lovato and X. Gong, "Phased antenna array beamforming using convolutional neural networks," in *Proc. IEEE Int. Symp. Antennas Propag. USNC-URSI Radio Sci. Meeting*, Atlanta, GA, USA, Jul. 2019, pp. 1247–1248.

[15] H. Huang, W. Xia, J. Xiong, J. Yang, G. Zheng, and X. Zhu, "Unsupervised learning-based fast beamforming design for downlink MIMO," *IEEE Access*, vol. 7, pp. 7599–7605, Dec. 2019.

[16] H. M. Yao, M. Li, and L. Jiang, "Applying deep learning approach to the far-field subwavelength imaging based on near-field resonant metalens at microwave frequencies," *IEEE Access*, vol. 7, pp. 63801–63808, 2019.

JAE HEE KIM (Senior Member, IEEE) received the B.S. degree in electrical engineering from Korea University, Seoul, South Korea, in 2005, and the Ph.D. degree in electrical engineering from the Pohang University of Science and Technology, Pohang, South Korea, in 2010. From 2010 to 2012, he was a Senior Engineer with Samsung Electronics, Suwon, South Korea. From 2012 to 2020, he was a Senior Researcher with the Korea Railroad Research Institute, Uiwang, South Korea. He is currently an Assistant Professor with the School of Electrical, Electronics and Communication Engineering, Korea University of Technology and Education, Cheonan, South Korea. His research interests include the design and analysis of antennas, microwave components, the development of wireless power transfer systems for railways, and the sensor fusion of autonomous vehicles

SANG WON CHOI (Member, IEEE) received the M.S. and Ph.D. degrees in electrical engineering and computer science from KAIST, Daejeon, South Korea, in 2004 and 2010, respectively. From February 2010 to March 2014, he was a Senior Research Engineer with Samsung Electronics for the development of multimode modem chips. From April 2014 to August 2020, he was a Senior Researcher with the Train Control and Communication Research Team, Korea Railroad Research Institute. Since September 2020, he has been an Assistant Professor with the Department of Electronic Engineering, Kyonggi University, South Korea. His research interests include mission-critical communications, mobile communication, communication signal processing, multi-user information theory, and machine learning. He was a recipient of the Silver Prize with the Samsung Humantech Paper Contest, in 2010.